J Eng Math (2009) 65:201–220
DOI 10.1007/s10665-009-9292-0

Adjoint-based optimization of thermo-fluid phenomena in welding processes

Oleg Volkov · Bartosz Protas · Wenyuan Liao · Donn W. Glander

Received: 30 March 2007 / Accepted: 2 April 2009 / Published online: 21 April 2009

Abstract A method is developed for optimizing the complex thermo-fluid phenomena that occur in welding processes where fluid convection is present. A mathematical model of a typical welding problem which includes conservation of mass, momentum and energy, and assumes that the process is steady in the frame of reference moving with the heat source is considered. An optimal control problem in which the heat input from the heat source is determined to ensure a prescribed geometry of the weld is formulated and solved. The problem is solved with a gradient-based optimization approach in which the gradient (sensitivity) of the cost functional with respect to the control variables is determined using a suitably defined adjoint system. An important aspect of the problem is that it is of the free-boundary type. Therefore it is necessary to use methods of the shape calculus to derive the adjoint equations. A number of computational results which validate our approach and feature qualitatively different flow patterns in problems with different material properties are presented.

Keywords Adjoint equations · Fluid mechanics · Free-boundary problems · Optimization · Welding

1 Introduction

Welding remains one of the most common joining processes in manufacturing. Joining of two workpieces occurs as a result of solidification of the metal molten in the neighborhood of the contact area following application of a heat source, such as a plasma arc, electric current, laser beam, liquid filler droplets, etc. [1, pp. 228–273]. Thus, the mechanical properties of the resulting joint, such as its strength, uniformity, resistance to fatigue, etc., are determined

O. Volkov · B. Protas (✉) · W. Liao
Department of Mathematics & Statistics, McMaster University, Hamilton, ON, Canada
e-mail: bprotas@mcmaster.ca

O. Volkov
e-mail: ovolkov@math.mcmaster.ca

W. Liao
e-mail: wyliao@math.mcmaster.ca

D. W. Glander
General Motors Research & Development Center,
Warren, MI, USA
e-mail: dwglander@yahoo.com

by the complex thermo-fluid phenomena occurring in the weld pool. It appears therefore plausible that modifying these phenomena by adjusting parameters of the heat source may lead to welds with more desirable properties. Optimization approaches are now routinely used in various areas of science and engineering; however, despite the ubiquity of welding in modern industry, few attempts have been made at rigorous and systematic optimization of welding processes (e.g., [2]). This seems due to the great complexity of the mathematical models describing the thermo-fluid phenomena occurring in such processes. An exception are approaches, such as in [3], based on genetic algorithms and neural networks which treat the physical system as a "black box" and hence do not really exploit the structure of the mathematical model. However, practitioners generally resort to ad-hoc trial and error methods in order to "optimize" various aspects of the welding process. Interestingly, optimization methods have found some application in determining unknown parameters of a welding process, thereby improving reliability of the modelling [4]. Methods of optimal control have also been applied to the related problem of solidification of alloys by Zabaras (see [5] for a review) and Hinze and Ziegenbalg [6]. In recent years important developments have been made pertaining to the modeling and prediction of the behavior of weld pools under different conditions based on first principles [7, pp. 21–76]. This also includes three-dimensional (3D) time-dependent problems involving transient phenomena (e.g., [8,9]). At the same time, significant advances were also made in application of rigorous methods of the Optimization Theory to solve control problem in fluid mechanics, such as drag reduction in open and closed flows [10], data assimilation in numerical weather prediction [11, pp. 136–204] and jet-noise reduction [12] to mention just a few. The reader is referred to the monograph [13] for a broad and up-to-date overview. Integration of advances in these two areas offers the promise of a rigorous optimization of welding processes. Since models of welding phenomena contain ingredients making their optimization significantly more complicated than for other flow problems, the goal of this paper is to address some of these issues.

An optimal control problem consists in determining inputs for a system, e.g., boundary or initial conditions, forcing, etc., such that the system evolution is optimal is some suitably defined sense. Hence, these problems belong to the category of *inverse problems* which in practice are often solved computationally using optimization methods. These approaches determine the optimal control input $\hat{\phi}$ and the corresponding optimal state $\hat{\mathbf{u}}$ as minimizers of a suitable cost functional $j(\phi, \mathbf{u})$ which measures the misfit between the actual and desired system output

$$(\hat{\phi}, \hat{\mathbf{u}}) = \operatorname{argmin}_{\phi\in\mathcal{U},\, \mathbf{u}\in\mathcal{X}} j(\phi, \mathbf{u}), \tag{1a}$$

$$\text{subject to } \mathcal{G}(\phi, \mathbf{u}) = 0, \tag{1b}$$

where $\mathcal{U}$ and $\mathcal{X}$ are, respectively, the space of admissible controls and the state space, both of which will be assumed to be equipped with a Hilbert structure, whereas $\mathcal{G}(\phi, \mathbf{u}) = 0$ represents the equation of state [usually a system of coupled partial differential equations (PDEs)]. Relations (1) represent a *constrained* optimization problem; however, in the presence of equality constraints only, such as (1b), and subject to suitable differentiability assumptions, we can write $\mathbf{u} = \mathbf{u}(\phi)$. This allows us to transform (1) into the corresponding *unconstrained* formulation by introducing a reduced cost functional $\mathcal{J}(\phi) \triangleq j(\phi, \mathbf{u}(\phi))$ ("$\triangleq$" means equality by definition). This approach thus yields

$$\hat{\phi} = \operatorname{argmin}_{\phi\in\mathcal{U}} \mathcal{J}(\phi). \tag{2}$$

Since this unconstrained formulation involves optimization with respect to ϕ only, it is usually more efficient from the computational point of view and hereafter we will focus on this approach exclusively (for brevity we will omit the term "reduced"). As regards computational solution of PDE-constrained optimization problems such as (1) and (2), there are two main paradigms referred to as "discretize-then-optimize" and "optimize-then-discretize". The relative merits of the two approaches are still a matter of debate [13, pp. 57–62]. In our investigation we will focus on the "optimize-then-discretize" approach which, while being perhaps less direct from a computational point of view, is more general in that it does not depend on the specific discretization used and is moreover more closely related to the actual physical problem.

The minimizer $\hat{\phi}$ is characterized by the first-order optimality condition requiring that the Gâteaux differential $\mathcal{J}'(\phi; \phi') \triangleq \lim_{\varepsilon\to 0} \frac{1}{\varepsilon}\left[\mathcal{J}(\phi + \varepsilon\phi') - \mathcal{J}(\phi)\right]$ of the cost functional computed at $\hat{\phi}$ should vanish for all admissible perturbations $\phi' \in \mathcal{U}$, i.e.,

$$\mathcal{J}'(\hat{\phi}; \phi') = 0, \quad \forall_{\phi'\in\mathcal{U}}. \tag{3}$$

As regards differentials, we will follow the convention that the quantity given after the semicolon represents the direction in which the differential is calculated. In fact, relation (3) is only a necessary condition. Sufficient conditions would require the use of second-order differentials which for problems governed by models as complicated as the one we will employ can be difficult to derive and compute numerically. Therefore, second-order conditions will not be considered here. An iterative solution of an optimal control problem (2)–(3) can be expressed as the following discrete initial-value problem in the control space $\mathcal{U}$

$$\begin{cases} \phi^{(n+1)} = \phi^{(n)} - \tau^{(n)} \nabla \mathcal{J}(\phi^{(n)}), \\ \phi^{(1)} \quad\;\; = \phi_0, \end{cases} \tag{4}$$

where $\phi^{(n)}, n = 1, \ldots$, are the consecutive approximations of the minimizer with the superscripts denoting the iterations and ϕ_0 is the initial guess. Equation 4 is solved until a critical point is reached, i.e., condition (3) is attained. Formulation (4) corresponds to the steepest descent algorithm with $\tau^{(n)}, n = 1, \ldots$, representing the step size chosen for every n as $\tau^{(n)} = \text{argmin}_\tau \, \mathcal{J}(\phi^{(n)} - \tau \nabla \mathcal{J}(\phi^{(n)}))$. Replacing $\tau^{(n)} \nabla \mathcal{J}(\phi^{(n)})$ with an expression of the form $\mathcal{A}_n \nabla \mathcal{J}(\phi) + \mathcal{B}_n$, we can obtain any of the gradient algorithms used in practice, such as the conjugate gradients or the quasi-Newton method [14, pp. 135–162]. Thus, calculation of the gradient $\nabla \mathcal{J}$ emerges as a crucial element of all gradient-based optimization algorithms and the present investigation explains how this can be accomplished for our model of the welding problem. We emphasize that the gradient $\nabla \mathcal{J}$ represents the *sensitivity* of the cost-functional $\mathcal{J}(\phi)$ to infinitesimal perturbations of the control ϕ in the presence of a constraint $\mathcal{G}(\phi, \mathbf{u}) = 0$. Hence, for a problem in which the control ϕ is a function of space and/or time, the gradient $\nabla \mathcal{J}$ is also a function of space and/or time, and the problem is therefore infinite-dimensional.

In a general welding process, the state of the system $\mathbf{u}(\phi)$ is the result of an interplay of the following physical phenomena:

(a) heat conduction with change of phase (melting and solidification of the metal in the weld pool),
(b) liquid-metal convection with a free surface,
(c) buoyancy effects related to the difference in densities between the different phases (Boussinesq effect),
(d) surface-tension-driven convection (Marangoni effect),
(e) electromagnetic (Lorentz) forces due to the presence of electromagnetic induction,
(f) interaction of the free surface with the heat source (electric arc, plasma, etc.),
(g) mass transfer into the weld pool (e.g., via impinging droplets).

In the literature there is still some debate concerning which of the effects (a)–(g) are most important for reliable modeling of different welding processes. In the present investigation we will focus solely on processes involving fluid convection in the weld pool, such as Metal Gas Inert (MIG) welding [1, Sect. 7.1.1]. From the mathematical optimization point of view, a crucial feature of this problem is that the geometry of the fluid domain depends on the control input and as such must be regarded as a *dependent variable*. As will become apparent in the sequel, this will have important ramifications for the calculation of the gradient $\nabla \mathcal{J}$. Our goal in this investigation is to establish a generic framework that, from a mathematical point of view, accounts for the most important ingredients of the problem. Such a template can then be adopted for a specific welding problem by incorporating appropriate effects from amongst (a)–(g), and choosing a correct model of the heat source. In order to derive such a general and versatile framework, we choose to include in our mathematical model effects (a), (b), (d) and (f) with a rather simple model of the heat source. For the sake of simplicity of this generic model and in view the problem-dependent nature of the phenomenon, the control will not involve mass transfer from the electrode to the weld pool. In general, one can consider two distinct regimes as regards the modelling of welding processes:

– the *transient regime* occurring during the initial and terminal phases when the heat source accelerates/decelerates and is close to one of the edges of the workpiece; in such conditions transient phenomena play a non-negligible role,
– the intermediate *steady regime* occurring when the heat source is travelling with a constant velocity along the joint and is at a large distance from the edges of the workpiece; assuming that the characteristic time of displacement of the heat source is much longer than the characteristic time of melting and solidification, in such

conditions the process may be considered statistically steady in the frame of reference attached to the travelling heat source.

In the present investigation we focus solely on the steady regime in which the mathematical model may be assumed time-independent resulting in a significant simplification of the solution of the inverse problem. The more general and challenging problem of optimization of a welding process in the transient regime will be studied next (in fact, some preliminary results concerning this problem obtained with a simple one-dimensional model were already reported in [15]). Therefore, our goal in this work is to determine an optimal spatial distribution of the heat input that will result in a steady (in the moving frame of reference) weld pool with a prescribed shape.

We emphasize that a main theme in this investigation is development of a gradient-based optimization algorithm in the form (4), so a large amount of our attention will be devoted to identifying the structure of the gradient $\nabla \mathcal{J}$ in terms of the variables of the problem. As a result, all our manipulations will be formal, i.e., they will implicitly assume that all underlying functions are regular enough to ensure well-posedness of all transformations. The important issue of proving existence, uniqueness and sufficient regularity of the relevant fields is outside the scope of this paper and has been addressed elsewhere for similar, yet much simpler, problems [16, Chap. 2].

The structure of the paper is as follows: in the next section we introduce the system of partial differential equations that will serve as our model for the typical thermo-fluid phenomena occurring in the weld pool; there we will also state the specific control problem that we want to solve; in Sect. 3 we identify the cost functional gradients using solutions of a suitably defined adjoint system; in the next section we present and discuss computational results; final conclusions will be given in Sect. 5.

2 Mathematical model of a generic welding process

In this section we define a mathematical model of a typical steady-state welding process in a form amenable to treatment as an optimization problem. In addition to stating the governing equations with appropriate boundary conditions, this also requires specification of the subdomains on which different parts of the model are formulated. The coordinate system is attached to the electrode (Fig. 1a) which travels with a constant velocity $\mathbf{v}_0 = U\,\mathbf{e}_y$, where U is a parameter and $\mathbf{e}_y$ is the unit vector aligned with the OY-axis.

2.1 Domains

As shown in Fig. 1, the domain of interest $\Omega \subset \mathbb{R}^3$ can be subdivided into the following two subdomains

$$\Omega = \Omega_L \cup \Omega_S, \tag{5}$$

where Ω_L refers to the part of the domain containing the liquid phase, whereas Ω_S refers to the part of the domain containing the solid phase. The boundaries of the domains will be denoted by $\partial\Omega_L$ and $\partial\Omega_S$. We also define the

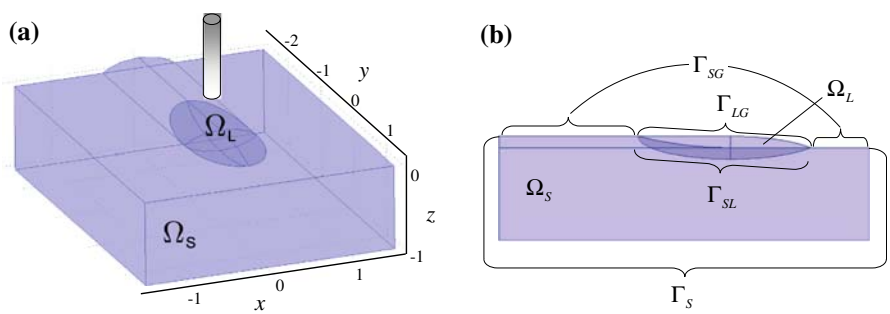

Fig. 1 Schematic of the problem geometry: (**a**) panoramic sketch and (**b**) longitudinal cross-section of the workpiece with the weld pool. In (**a**) the vertical cylinder represents the heat source (electrode)

solid–liquid interface as $\Gamma_{SL} \triangleq \partial\Omega_S \cap \partial\Omega_L$ as the boundary between Ω_S and Ω_L. The free surface of the liquid domain (i.e., the liquid–gas interface) will be denoted by Γ_{LG}, so that $\partial\Omega_L = \Gamma_{SL} \cup \Gamma_{LG}$. The boundary of the solid subdomain Ω_S will consist of three parts: the solid–liquid interface Γ_{SL}, the top surface Γ_{SG} and the surfaces Γ_S representing the far-field boundary, so that $\partial\Omega_S = \Gamma_{SL} \cup \Gamma_{SG} \cup \Gamma_S$. Without loss of generality, we will assume that the unit normal vector $\mathbf{n}$ points into Ω_L on the interfaces Γ_{SL} and Γ_{LG}, and out of Ω_S on the interface Γ_{SG}. Hereafter we will employ the convention that, when stating generally valid relations, we will drop the subscripts from the symbols denoting domains and interfaces. On the other hand, we will retain the subscripts in expressions valid in a specific domain or on a specific interface only.

2.2 Conservation equations

Given the assumptions made in Sect. 1 regarding the physical effects to be accounted for in the model and the assumption of steadiness in the moving frame of reference, we consider the following dependent variables:

- velocity $\mathbf{v} = [u, v, w] : \Omega_L \to \mathbb{R}^3$,
- pressure $p : \Omega_L \to \mathbb{R}$,
- temperature $T : \Omega \to \mathbb{R}$,
- position of the free surface $\Gamma_{LG} \in \mathbb{S}^2$,

where $\mathbb{S}^2$ is a set of smooth two-dimensional surfaces contained in $\mathbb{R}^3$. We emphasize that the position of the solid–liquid interface Γ_{SL} is not a dependent variable, but is instead imposed as a constraint chosen to represent the engineering objective of an optimal penetration depth of the weld pool. The intersection of the two interfaces Γ_{SL} and Γ_{LG} forms the *contact line* $\delta \triangleq \overline{\Gamma}_{SL} \cap \overline{\Gamma}_{LG}$. Now we proceed to derive the governing equations in the moving frame of reference. Let $\mathbf{x}$ and $\tilde{\mathbf{x}}$ denote the position vectors in the moving and fixed coordinate systems, respectively. Then, the velocities and temperatures in the two coordinate systems are related as follows

$$T(\mathbf{x}) = T(\tilde{\mathbf{x}} - t\,\mathbf{v}_0) \triangleq \tilde{T}(t, \tilde{\mathbf{x}}), \tag{6a}$$

$$\mathbf{v}(\mathbf{x}) = \mathbf{v}(\tilde{\mathbf{x}} - t\,\mathbf{v}_0) \triangleq \tilde{\mathbf{v}}(t, \tilde{\mathbf{x}}), \tag{6b}$$

where the quantities with the tildes ($\tilde{}$) are defined in the fixed coordinate system. The assumed steadiness in the moving frame of reference implies that the time-derivative terms transform as follows

$$\left.\frac{\partial \tilde{T}}{\partial t}\right|_{\mathbf{x}=\text{const}} = -\mathbf{v}_0 \cdot \nabla T, \tag{7a}$$

$$\left.\frac{\partial \tilde{\mathbf{v}}}{\partial t}\right|_{\mathbf{x}=\text{const}} = -\mathbf{v}_0 \cdot \nabla \mathbf{v}, \tag{7b}$$

where the operator ∇ involves differentiation with respect to $\mathbf{x}$. Thus, the process in the steady-state regime is modelled by the following system of equations

$$\rho\,(\mathbf{v} - \mathbf{v}_0) \cdot \nabla \mathbf{v} - \nabla \cdot \boldsymbol{\sigma} - \rho \mathbf{g} = 0 \quad \text{in } \Omega_L, \tag{8a}$$

$$\nabla \cdot \mathbf{v} = 0 \quad \text{in } \Omega_L, \tag{8b}$$

$$(\mathbf{v} - \mathbf{v}_0) \cdot \nabla T - \nabla \cdot (k_L \nabla T) = 0 \quad \text{in } \Omega_L, \tag{8c}$$

$$-\mathbf{v}_0 \cdot \nabla T - \nabla \cdot (k_S \nabla T) = 0 \quad \text{in } \Omega_S, \tag{8d}$$

where ρ is the density of the liquid metal (assumed constant), $\boldsymbol{\sigma} \triangleq -p\,\mathbf{I} + \mu\left[\nabla \mathbf{v} + (\nabla \mathbf{v}^T)\right]$ is the stress tensor in which $\mathbf{I}$ is the identity matrix and μ the dynamic viscosity, whereas $\mathbf{g} = (0, 0, g_z)^T$ is the gravitational acceleration. The coefficients k_L and k_S represent the thermal diffusivities of the liquid and solid phases. We note that Eqs. 8a and 8b represent conservation of mass and momentum, whereas Eqs. 8c and 8d represent conservation of energy in the respective domains.

2.3 Boundary conditions

System (8) involves PDEs and therefore must be supplemented with boundary conditions for the velocity $\mathbf{v}$ and for the temperature T.

2.3.1 Boundary conditions on the solid–liquid interface Γ_{SL}

The velocity satisfies the no-slip (Dirichlet) boundary condition implying that $\mathbf{v}$ is equal to the velocity of the boundary, i.e.,

$$\mathbf{v} = \mathbf{v}_0 \quad \text{on } \Gamma_{SL}. \tag{9}$$

As regards the boundary conditions for the energy equations (8c) and (8d), they require the temperature to be continuous across the interface and satisfy the Stefan flux condition [17, Sect. 5.1], i.e.,

$$T_S = T_L \quad \text{on } \Gamma_{SL}, \tag{10a}$$

$$-\left[k\frac{\partial T}{\partial n}\right]_S^L = L(\mathbf{v}_0 \cdot \mathbf{n}) \quad \text{on } \Gamma_{SL}, \tag{10b}$$

where L is the latent heat of solidification and melting, where the expression $[\circ]_S^L$ denotes the jump of the given quantity across an interface (here Γ_{SL}).

2.3.2 Boundary conditions on the liquid–gas interface Γ_{LG}

The liquid–gas interface is of the free-surface type and the boundary conditions for the momentum equation express the balance between the stress in the fluid and the surface tension. We note that the surface tension f is an empirical property of the material which is usually modelled as a linear function of the temperature T, i.e.,

$$f(T) = f_m^0 + A(T - T_m), \tag{11}$$

where f_m^0 is the surface tension at the melting temperature T_m and A is a constant. As regards the energy equation, we prescribe the Neumann data for the temperature in terms of the space-dependent heat flux φ due to the heat source. Thus, we obtain

$$[\boldsymbol{\sigma}]_G^L \cdot \mathbf{n} = f(T)\,\kappa\mathbf{n} - \nabla_\Gamma f(T) \quad \text{on } \Gamma_{LG}, \tag{12a}$$

$$k_L \frac{\partial T}{\partial n}\bigg|_L = \varphi \quad \text{on } \Gamma_{LG}, \tag{12b}$$

where $\kappa \triangleq \nabla \cdot \mathbf{n}$ is the mean curvature and $\nabla_\Gamma \triangleq \nabla - \mathbf{n}\frac{\partial}{\partial n}$ is the surface gradient [21, Chap. 8]. On the gas side there are no viscous stresses, and the stress tensor is given in terms of the ambient pressure p_a only, i.e., $\boldsymbol{\sigma}_G = -p_a\mathbf{I}$. We reiterate that the position of the interface Γ_{SL} is also unknown and must be found as part of the solution to the problem.

2.3.3 Boundary conditions on the solid–gas interface Γ_{SG}

On the boundary Γ_{SG} we only need to prescribe the boundary condition for the energy equation (8d), and choose an analogous expression as on Γ_{LG} [cf. (12b)], i.e.,

$$k_S \frac{\partial T}{\partial n}\bigg|_S = \varphi \quad \text{on } \Gamma_{SG}. \tag{13}$$

We emphasize that the function $\varphi : \Gamma_{LG} \cup \Gamma_{SG} \to \mathbb{R}$ represents in fact the control input we seek to optimize.

2.3.4 Far-field boundary conditions on Γ_S

On the far-field boundary Γ_S we need to prescribe the boundary condition for energy equation (8d) only, and assume that the temperature is equal to the ambient temperature T_a there, i.e.,

$$T = T_a \quad \text{on } \Gamma_S. \tag{14}$$

We conclude that a complete description of our typical steady-state welding problem is thus provided by system of equations (8) together with boundary conditions (9)–(14).

2.4 Cost functional

In this subsection we introduce the specific cost functional that we want to minimize. As mentioned in the introduction, engineering objectives in welding problems are usually related to the optimal shape of a weld joint after solidification, which is to be obtained using the least possible amount of the thermal input. Therefore, our cost functional is chosen so that its minimizers will be the optimal heat input distribution φ and the position of the free surface Γ_{LG} which result in a steady-state weld pool with a prescribed geometry of the solid–liquid interface Γ_{SL}

$$\begin{aligned}\mathcal{J}(\varphi, \Gamma_{LG}) &= \frac{\gamma_1}{2}\int_{\Gamma_{SL}} (T - T_m)^2 \,\mathrm{d}s + \frac{\gamma_2}{2}\int_{\Gamma_{LG}} V^2 \,\mathrm{d}s + \frac{\gamma_3}{2}\int_{\Gamma_{LG}\cup\Gamma_{SG}} \varphi^2 \,\mathrm{d}s + \frac{\gamma_4}{2}\left(\int_{\Omega_L} \mathrm{d}x - \mathrm{Vol}_L\right)^2 \\ &\triangleq \gamma_1\mathcal{J}_1 + \gamma_2\mathcal{J}_2 + \gamma_3\mathcal{J}_3 + \gamma_4\mathcal{J}_4,\end{aligned} \tag{15}$$

where $V \triangleq (\mathbf{v} - \mathbf{v}_0)\cdot\mathbf{n}$. The term $\mathcal{J}_1$ ensures that the interface Γ_{SL} is in fact a phase-change (Stefan) boundary, whereas the term $\mathcal{J}_2$ guarantees the steadiness of the free surface Γ_{LG}. The thermodynamic and mathematical justification for these two terms was analyzed in detail in [17]; see also [18] for a more general discussion. The term $\mathcal{J}_3$ ensures the energetic efficiency of the process by penalizing the $L_2(\Gamma_{LG}\cup\Gamma_{SG})$ norm of the heat input, and can also be interpreted as the Tikhonov regularization necessary for the mathematical well-posedness of the problem [19, pp. 241–276]. The term $\mathcal{J}_4$ guarantees that the volume of the weld pool is close to the prescribed value Vol_L, and therefore could be used to account for the mass transfer into the weld pool. The parameters γ_1, γ_2, γ_3, and γ_4 are used to adjust the relative significance of the different terms. We note that the control variable φ represents the actual solution of the inverse problem we are interested in. On the other hand, the second control variable (the position of the interface Γ_{LG}) serves as an auxiliary variable allowing us to determine the location of the free boundary via an optimization process. We found this to be a convenient alternative to other ways of computing free boundaries. Thus, our optimization problem is given by (2) with $\phi = \{\varphi, \Gamma_{LG}\}$ and cost functional (15).

3 Characterization of the cost-functional gradients

In this section we derive expressions for the gradients $\nabla_\varphi\mathcal{J}$ and $\nabla_{\Gamma_{LG}}\mathcal{J}$ of cost functional (15) with respect to the heat flux φ and the position of the liquid–gas interface Γ_{LG}. We will derive those expressions using suitably defined *adjoint* variables. A distinguishing feature of the problem described by (8)–(14) is that it is of the free-boundary type, since the shape of the domain Ω_L, more specifically its boundary Γ_{LG}, needs to be determined as a part of the solution of the problem. This fact has important consequences for how the differentials of the state variables are calculated with respect to the control variables φ and Γ_{SL}. The general framework for differentiation of solutions of PDEs with respect to the shape of the domain is provided by the "shape calculus" whose main results are reviewed in the monographs [20–22], whereas some applications to problems in fluid mechanics are surveyed in [23]. Below we review the main elements of the shape-differential calculus relevant for the present problem, and refer the reader to the aforementioned monographs for further mathematical details.

3.1 Elements of the shape calculus

When defining differentiation with respect to the shape of the domain the key challenge is a suitable parametrization of the geometry. In the shape calculus perturbations of the boundary (interface) geometry can be represented as

$$\mathbf{x}(\tau, \mathbf{x}') = \mathbf{x} + \tau \mathbf{x}' \quad \text{for } \mathbf{x} \in \Gamma(0), \tag{16}$$

where τ is a real parameter, $\Gamma(0)$ is the original unperturbed boundary and $\mathbf{x}' : \Omega \to \mathbb{R}^2$ is a "velocity" field characterizing the perturbation. The points $\mathbf{x}(\tau, \mathbf{x}')$ thus define the perturbed boundary $\Gamma(\tau, \mathbf{x}')$ (an expression analogous to (16) could also be written for $\Omega(\tau, \mathbf{x}')$, but is omitted here for brevity). We will use the notation $\Omega(0) \triangleq \Omega(0, \mathbf{x}')$ and $\Gamma(0) \triangleq \Gamma(0, \mathbf{x}')$ (with suitable subscripts) for domains and their boundaries, respectively. The Gâteaux shape differential of a functional such as (15) with respect to the shape of the interface Γ_{LG} and computed in the direction of the perturbation field $\mathbf{x}'$ is thus defined as

$$\mathcal{J}'(\Gamma_{SL}(0); \mathbf{x}') \triangleq \lim_{\tau \to 0} \frac{\mathcal{J}(\Gamma_{SL}(\tau, \mathbf{x}')) - \mathcal{J}(\Gamma_{SL}(0))}{\tau}. \tag{17}$$

Given cost functional (15), its shape differential (17) can be computed using a classical result concerning shape differentiation [24] which says that for a smooth domain $\Omega(\tau, \mathbf{x}')$ and smooth functions F and G defined, respectively, on this domain and its boundary we have

$$\left(\int_{\Omega(\tau, \mathbf{x}')} F \, \mathrm{d}\Omega + \int_{\partial\Omega(\tau, \mathbf{x}')} G \, \mathrm{d}s \right)' = \int_{\Omega(0)} F' \, \mathrm{d}\Omega + \int_{\partial\Omega(0)} G' \, \mathrm{d}s + \int_{\partial\Omega(0)} \left(F + \kappa G + \frac{\partial G}{\partial n} \right) \mathbf{x}' \cdot \mathbf{n} \, \mathrm{d}s, \tag{18}$$

where a prime denotes the shape derivative defined as in (17) and $\mathbf{n}$ is the unit normal vector pointing out of the domain Ω.

3.2 Differential of the cost functional

In order to identify the gradients (sensitivities) $\nabla_{\varphi} \mathcal{J}$ and $\nabla_{\Gamma_{LG}} \mathcal{J}$ of cost functional (15) with respect to the control variables $\{\varphi, \Gamma_{LG}\}$, one must first obtain an expression for the Gâteaux directional derivative of $\mathcal{J}$ with respect to these variables. We do this by combining standard differentiation with the shape differentiation described in Sect. 3.1 which yields

$$\begin{aligned} \mathcal{J}'(\varphi, \Gamma_{LG}; \varphi', \mathbf{x}') = {} & \gamma_1 \int_{\Gamma_{SL}} (T - T_m) \, T' \, \mathrm{d}s + \gamma_2 \int_{\Gamma_{LG}} V \, (\mathbf{v}' \cdot \mathbf{n}) \, \mathrm{d}s \\ & + \int_{\Gamma_{LG}} \left[\gamma_2 \left(\frac{\kappa}{2} V^2 + V \frac{\partial V}{\partial n} \right) + \gamma_4 \left(\int_{\Omega_L} \mathrm{d}x - \mathrm{Vol}_L \right) \right] (\mathbf{x}' \cdot \mathbf{n}) \, \mathrm{d}s \\ & - \gamma_2 \int_{\Gamma_{LG}} V \, (\mathbf{v} - \mathbf{v}_0) \cdot \nabla_{\Gamma} (\mathbf{x}' \cdot \mathbf{n}) \, \mathrm{d}s + \gamma_3 \int_{\Gamma_{LG} \cup \Gamma_{SG}} \varphi \, \varphi' \, \mathrm{d}s, \end{aligned} \tag{19}$$

where φ' and $\mathbf{x}'$ denote perturbations of the control variables. Without loss of generality, we will assume that the perturbations of the boundary have a normal component only, i.e., $\mathbf{x}' \triangleq \zeta' \mathbf{n}$, where $\zeta' : \Gamma_{LG} \to \mathbb{R}$ [21, pp. 350–360]. This assumption, which will simplify the form of the ultimate result, follows from the fact that the tangential components of the perturbation $\mathbf{x}'$ do not change the shape of the boundary when the contact line δ is fixed. Considering Gâteaux differential (19) as a bounded linear functional with respect to $\{\varphi', \zeta'\}$, and invoking Riesz's theorem [25, pp. 30–31] will allow us to extract the cost functional gradients $\nabla_{\varphi} \mathcal{J} : \Gamma_{LG} \cup \Gamma_{SG} \to \mathbb{R}$ and $\nabla_{\Gamma_{LG}} \mathcal{J} : \Gamma_{LG} \to \mathbb{R}$ using the following identity

$$\mathcal{J}'(\varphi, \Gamma_{LG}; \varphi', \zeta' \mathbf{n}) = \left\langle \begin{bmatrix} \nabla_{\varphi} \mathcal{J} \\ \nabla_{\Gamma_{LG}} \mathcal{J} \end{bmatrix}, \begin{bmatrix} \varphi' \\ \zeta' \end{bmatrix} \right\rangle_{L_2} = \int_{\Gamma_{LG} \cup \Gamma_{SG}} (\nabla_{\varphi} \mathcal{J}) \varphi' \, \mathrm{d}s + \int_{\Gamma_{LG}} (\nabla_{\Gamma_{LG}} \mathcal{J}) \zeta' \, \mathrm{d}s, \tag{20}$$

where, for simplicity, the L_2 inner product was used [27]. We emphasize that the gradient with respect to the heat flux is defined on the entire top surface, not only on the free boundary Γ_{LG}. We note that relation (19) contains terms which are already in the Riesz form with the perturbations $\mathbf{x}'$ and φ' appearing as factors, but it also includes terms involving perturbations of the other state variables, namely, $\mathbf{v}'$, p' and T'. Because of the presence of these latter terms, at this stage we cannot use relation (19) to identify the gradients $\nabla_{\varphi}\mathcal{J}$ and $\nabla_{\Gamma_{LG}}\mathcal{J}$. Therefore, our goal in the following section will be to use suitably defined adjoint variables to transform the remaining part of expression (19) into a form consistent with Riesz's representation (20).

3.3 Adjoint system

We begin by writing a weak form of system (8)–(14) for the variables $\mathbf{v} \in \{\mathbf{H}^1(\Omega_L) \,|\, \mathbf{v} = \mathbf{v}_0 \text{ on } \Gamma_{SL}\}$, $p \in L_2(\Omega_L)$, and $T \in \{H^1(\Omega_L \cup \Omega_S) \,|\, T = T_s \text{ on } \Gamma_S\}$

$$\int_{\Omega_L} [(\mathbf{v}-\mathbf{v}_0)\cdot\nabla T - \nabla\cdot(k_L\,\nabla T)]\; T^*\,\mathrm{d}x + \int_{\Omega_S} [(-\mathbf{v}_0)\cdot\nabla T - \nabla\cdot(k_S\,\nabla T)]\; T^*\,\mathrm{d}x$$
$$+ \int_{\Omega_L} \left[\rho\,(\mathbf{v}-\mathbf{v}_0)\cdot\nabla\mathbf{v} - \nabla\cdot\boldsymbol{\sigma} - \rho\,\mathbf{g}\right]\cdot\mathbf{v}^* - (\nabla\cdot\mathbf{v})\,p^*\,\mathrm{d}x = 0, \tag{21}$$

where H^1 and $\mathbf{H}^1$ denote the Sobolev spaces of, respectively, scalar-valued and vector-valued functions with square-integrable gradients [26, pp. 59–78], and we used the test functions $\mathbf{v}^* \in \{\mathbf{H}^1(\Omega_L) \,|\, \mathbf{v}^* = 0 \text{ on } \Gamma_{SL}\}$, $p^* \in L_2(\Omega_L)$, and $T^* \in \{H^1(\Omega_L \cup \Omega_S) \,|\, T^* = 0 \text{ on } \Gamma_S\}$ (these test functions will be in fact identified later on as the adjoint variables, hence we denote them with asterisks). After integrating the second-order terms by parts, relation (21) becomes

$$\int_{\Omega_L} T^*\,(\mathbf{v}-\mathbf{v}_0)\cdot\nabla T + k_L(\nabla T\cdot\nabla T^*)\,\mathrm{d}x + \int_{\Omega_S} T^*\;(-\mathbf{v}_0)\cdot\nabla T + k_S(\nabla\, T\cdot\nabla T^*)\,\mathrm{d}x$$
$$- \int_{\Gamma_{LG}} k_L\;\frac{\partial T}{\partial n}\bigg|_L\; T^*\,\mathrm{d}s - \int_{\Gamma_{SG}} k_S\;\frac{\partial T}{\partial n}\bigg|_S\; T^*\,\mathrm{d}s - \int_{\Gamma_{SL}} \left[k\,\frac{\partial T}{\partial n}\right]_S^L\; T^*\,\mathrm{d}s$$
$$+ \int_{\Omega_L} \left[\rho\,(\mathbf{v}-\mathbf{v}_0)\cdot\nabla\mathbf{v} - \rho\,\mathbf{g}\right]\cdot\mathbf{v}^* - (\nabla\cdot\mathbf{v}^*)\,p + \boldsymbol{\sigma}^* : \nabla\,\mathbf{v}\,\mathrm{d}x - \int_{\Gamma_{LG}} \mathbf{n}\cdot\boldsymbol{\sigma}\cdot\mathbf{v}^*\mathrm{d}s = 0, \tag{22}$$

where $\boldsymbol{\sigma}^* \triangleq -p^*\,\mathbf{I} + \mu\left[\nabla\mathbf{v}^* + (\nabla\mathbf{v}^*)^T\right]$ and the colon (:) denotes the scalar product (contraction) of two tensors defined as $\mathbf{A} : \mathbf{B} = \sum_{i,j=1}^{3} A_{i,j}\,B_{j,i}$. Using now boundary conditions (9)–(14), we may simplify the weak formulation (22) to

$$\int_{\Omega_L} T^*\,(\mathbf{v}-\mathbf{v}_0)\cdot\nabla T + k_L(\nabla T\cdot\nabla T^*)\,\mathrm{d}x - \int_{\Gamma_{SL}} L(\mathbf{v}_0\cdot\mathbf{n})\,T^*\,\mathrm{d}s + \int_{\Omega_S} T^*\;(-\mathbf{v}_0)\cdot\nabla T + k_S(\nabla\, T\cdot\nabla T^*)\,\mathrm{d}x$$
$$- \int_{\Gamma_{LG}\cup\Gamma_{SG}} T^*\,\varphi\,\mathrm{d}s + \int_{\Omega_L} \left[\rho\,(\mathbf{v}-\mathbf{v}_0)\cdot\nabla\mathbf{v} - \rho\,\mathbf{g}\right]\cdot\mathbf{v}^* - (\nabla\cdot\mathbf{v}^*)\,p + \boldsymbol{\sigma}^* : \nabla\,\mathbf{v}\,\mathrm{d}x + \int_{\partial\Omega_L} (\nabla_\Gamma\cdot\mathbf{v}^*)\,f\,\mathrm{d}s = 0, \tag{23}$$

where we also employed the following identity of the shape calculus [21]

$$\int_{\partial\Omega_L} \mathbf{v}^*\cdot(f\,\kappa\mathbf{n} - \nabla_\Gamma\, f)\;\mathrm{d}s = \int_{\partial\Omega_L} (\nabla_\Gamma\cdot\mathbf{v}^*)\,f\,\mathrm{d}s.$$

We now compute the variation of relation (23) with respect to the control variables $\{\varphi, \Gamma_{LG}\}$ in the direction given by the perturbations $\{\varphi', \mathbf{x}'\}$. We remark that perturbing with respect to the shape of the free boundary Γ_{LG} requires us to use shape-differentiation, more specifically, formula (18), and the result is

$$\int_{\Omega_L} T^* (\mathbf{v} - \mathbf{v}_0) \cdot \nabla T' + T^* \mathbf{v}' \cdot \nabla T + k_L (\nabla T' \cdot \nabla T^*) \, \mathrm{d}x + \int_{\Omega_S} T^* \, (-\mathbf{v}_0) \cdot \nabla T' + k_S (\nabla T' \cdot \nabla T^*) \, \mathrm{d}x$$
$$+ \int_{\partial\Omega_L} (\nabla_\Gamma \cdot \mathbf{v}^*) \frac{\mathrm{d}f}{\mathrm{d}T} T' \, \mathrm{d}s + \int_{\Omega_L} \left[\rho \, \mathbf{v}' \cdot \nabla \mathbf{v} + \rho \, (\mathbf{v} - \mathbf{v}_0) \cdot \nabla \mathbf{v}'\right] \cdot \mathbf{v}^* - (\nabla \cdot \mathbf{v}^*) \, p' + \boldsymbol{\sigma}^* : \nabla \mathbf{v}' \, \mathrm{d}x + I = 0 \quad (24)$$

in which we denoted

$$I \triangleq \int_{\Gamma_{LG}} \left[\nabla \cdot (\boldsymbol{\sigma} \cdot \mathbf{v}^*) + \kappa (\nabla_\Gamma \cdot \mathbf{v}^*) \, f + \frac{\partial}{\partial n} \left((\nabla_\Gamma \cdot \mathbf{v}^*) \, f\right) - (\nabla \cdot \mathbf{v}) \, p^*\right] (\mathbf{x}' \cdot \mathbf{n}) \, \mathrm{d}s$$
$$+ \int_{\Gamma_{LG}} \left[T^* (\mathbf{v} - \mathbf{v}_0) \cdot \nabla T + k_L \, \nabla_\Gamma T \cdot \nabla_\Gamma T^* - \kappa \varphi \, T^*\right] (\mathbf{x}' \cdot \mathbf{n}) \, \mathrm{d}s + \int_{\Gamma_{LG}} f \, \frac{\mathbf{n} \cdot \boldsymbol{\sigma}^*}{\mu} \cdot \nabla_\Gamma (\mathbf{x}' \cdot \mathbf{n}) \, \mathrm{d}s$$
$$- \int_{\Gamma_{LG} \cup \Gamma_{SG}} T^* \varphi' \, \mathrm{d}s. \quad (25)$$

We note that expression I collects only those terms in which the perturbations φ' and $\mathbf{x}'$ appear as factors. In (25) we denoted $\boldsymbol{\sigma} \cdot \mathbf{v}^* = \sum_{j=1}^{3} \boldsymbol{\sigma}_{i,j} v_j^*$, and used also the following identity of the shape calculus [21, p. 367]

$$(\nabla_\Gamma \cdot \mathbf{v})' = \left(\nabla_\Gamma \cdot \mathbf{v}'\right) + \mathbf{n} \cdot \left[\nabla \mathbf{v} + (\nabla \mathbf{v})^T\right] \cdot \nabla_\Gamma (\mathbf{x}' \cdot \mathbf{n}) + \left(\frac{\partial \nabla_\Gamma \cdot \mathbf{v}}{\partial n}\right) (\mathbf{x}' \cdot \mathbf{n})$$
$$= \left(\nabla_\Gamma \cdot \mathbf{v}'\right) + \frac{\mathbf{n} \cdot \boldsymbol{\sigma}}{\mu} \cdot \nabla_\Gamma (\mathbf{x}' \cdot \mathbf{n}) + \left(\frac{\partial \nabla_\Gamma \cdot \mathbf{v}}{\partial n}\right) (\mathbf{x}' \cdot \mathbf{n}). \quad (26)$$

As regards (26), we note that we could replace $\mathbf{n} \cdot \left[\nabla \mathbf{v} + (\nabla \mathbf{v})^T\right]$ with $\frac{1}{\mu} \mathbf{n} \cdot \boldsymbol{\sigma}$, because the pressure term is orthogonal to the tangential gradient $\nabla_\Gamma (\mathbf{x}' \cdot \mathbf{n})$, and therefore has no effect. We remark that the variation field T' might in general be discontinuous across the interface Γ_{SL}. However, after applying variations to boundary condition (10a) one obtains

$$\left[T'\right]_S^L = 0 \quad \text{on } \Gamma_{SL}. \quad (27)$$

Applying variations to the Dirichlet boundary conditions on the other fixed boundaries, i.e., relations (9) and (14), yields

$$\mathbf{v}' = 0 \quad \text{on } \Gamma_{SL}, \quad (28a)$$
$$T' = 0 \quad \text{on } \Gamma_S. \quad (28b)$$

As a next step we integrate expression (24) by parts which gives

$$\int_{\Omega_L} \left[-(\mathbf{v}-\mathbf{v}_0)\cdot\nabla T^* - \nabla\cdot(k_L\nabla T^*)\right] T'\,\mathrm{d}x + \int_{\Omega_S} \left[\mathbf{v}_0\cdot\nabla T^* - \nabla\cdot(k_S\nabla T^*)\right] T'\,\mathrm{d}x$$
$$+ \int_{\Gamma_S} k_S \left.\frac{\partial T^*}{\partial n}\right|_S T'\,\mathrm{d}s + \int_{\Gamma_{SG}} \left[k_S \left.\frac{\partial T^*}{\partial n}\right|_S - (\mathbf{v}_0\cdot\mathbf{n})\,T^*\right] T'\,\mathrm{d}s + \int_{\Gamma_{LG}} \left[k_L \left.\frac{\partial T^*}{\partial n}\right|_L + T^*\,(\mathbf{v}-\mathbf{v}_0)\cdot\mathbf{n}\right.$$
$$\left. + (\nabla_\Gamma\cdot\mathbf{v}^*)\,\mathrm{d}f(T)/\mathrm{d}T\right] T'\,\mathrm{d}s + \int_{\Gamma_{SL}} \left\{\left[k\,\frac{\partial T^*}{\partial n}\right]_S^L + (\mathbf{v}_0\cdot\mathbf{n})\,T^* + (\nabla_\Gamma\cdot\mathbf{v}^*)\,\mathrm{d}f(T)/\mathrm{d}T\right\} T'\mathrm{d}s$$
$$+ \int_{\Omega_L} \left[-\rho\,(\mathbf{v}-\mathbf{v}_0)\cdot\nabla\mathbf{v}^* + \rho\,\mathbf{v}^*\cdot(\nabla\mathbf{v})^T - \nabla\cdot\boldsymbol{\sigma}^* + T^*\,\nabla T\right]\cdot\mathbf{v}'\,\mathrm{d}x$$
$$+ \int_{\Gamma_{LG}\cup\Gamma_{SL}} \left(\rho\,V\,\mathbf{v}^* + \mathbf{n}\cdot\boldsymbol{\sigma}^*\right)\cdot\mathbf{v}'\,\mathrm{d}s - \int_{\Omega_L} (\nabla\cdot\mathbf{v}^*)\,p'\,\mathrm{d}x + I = 0. \tag{29}$$

We now observe that $\mathbf{v}^*$, p^* and T^* are the adjoint variables with respect to $\mathbf{v}$, p and T provided they satisfy the following *adjoint equations*

$$(\mathbf{v}_0-\mathbf{v})\cdot\nabla T^* = \nabla\cdot(k_L\,\nabla T^*) \quad \text{in } \Omega_L, \tag{30a}$$
$$\mathbf{v}_0\cdot\nabla T^* = \nabla\cdot(k_S\,\nabla T^*) \quad \text{in } \Omega_S, \tag{30b}$$
$$\rho\,(\mathbf{v}-\mathbf{v}_0)\cdot\nabla\mathbf{v}^* + \nabla\cdot\boldsymbol{\sigma}^* = \rho\,\mathbf{v}^*\cdot(\nabla\mathbf{v})^T + T^*\,\nabla T \quad \text{in } \Omega_L, \tag{30c}$$
$$\nabla\cdot\mathbf{v}^* = 0 \quad \text{in } \Omega_L \tag{30d}$$

supplied with the boundary conditions

$$\mathbf{n}\cdot\boldsymbol{\sigma}^* = -V\,(\rho\,\mathbf{v}^* + \gamma_2\,\mathbf{n}) \quad \text{on } \Gamma_{LG}, \tag{31a}$$
$$\mathbf{v}^* = 0 \quad \text{on } \Gamma_{SL}, \tag{31b}$$
$$k_L\,\frac{\partial T^*}{\partial n} + V\,T^* = -(\nabla_\Gamma\cdot\mathbf{v}^*)\,\mathrm{d}f(T)/\mathrm{d}T \quad \text{on } \Gamma_{LG}, \tag{31c}$$
$$k_S\,\frac{\partial T^*}{\partial n} - (\mathbf{v}_0\cdot\mathbf{n})\,T^* = 0 \quad \text{on } \Gamma_{SG}, \tag{31d}$$
$$\left[k\,\frac{\partial T^*}{\partial n}\right]_S^L + (\mathbf{v}_0\cdot\mathbf{n})\,T^* = -\gamma_1\,(T-T_m) \quad \text{on } \Gamma_{SL}, \tag{31e}$$
$$T^* = 0 \quad \text{on } \Gamma_S. \tag{31f}$$

Using relations (27) and (28), together with the definition of the adjoint system in (30) and (31), allows us to simplify expression (29), so that we obtain

$$I = \gamma_1 \int_{\Gamma_{SL}} (T-T_m)\,T'\,\mathrm{d}s + \gamma_2 \int_{\Gamma_{LG}} V\,(\mathbf{v}'\cdot\mathbf{n})\,\mathrm{d}s. \tag{32}$$

On the right-hand side of (32) one recognizes two terms from expression (19) for the variation $\mathcal{J}'(\varphi, \Gamma_{LG}; \varphi', \mathbf{x}')$, whereas expression (25) appearing on the left-hand side is already in the desired form with the perturbations φ' and $\mathbf{x}'$ entering as factors. Indeed, after substituting (32) in expression (19) we get

$$\mathcal{J}'(\varphi,\Gamma_{LG};\varphi',\mathbf{x}') = \int\limits_{\Gamma_{LG}\cup\Gamma_{SG}} \left(\gamma_3\,\varphi - T^*\right)\,\varphi'\,\mathrm{d}s + \int\limits_{\Gamma_{LG}} \Bigg[\nabla\cdot(\boldsymbol{\sigma}\cdot\mathbf{v}^*) + \kappa(\nabla_\Gamma\cdot\mathbf{v}^*)\,f + \frac{\partial}{\partial n}\left(\left(\nabla_\Gamma\cdot\mathbf{v}^*\right)\,f\right)$$
$$+ T^*\,(\mathbf{v}-\mathbf{v}_0)\cdot\nabla T + k_L\,\nabla_\Gamma T\cdot\nabla_\Gamma T^* - \kappa\varphi\,T^* + \gamma_3\frac{\kappa\varphi^2}{2} + \gamma_2\,V\left(\frac{\kappa V}{2}+\frac{\partial V}{\partial n}\right)$$
$$+ \gamma_4\left(\int\limits_{\Omega_L}\mathrm{d}x - \mathrm{Vol}_L\right)\Bigg](\mathbf{x}'\cdot\mathbf{n})\,\mathrm{d}s - \int\limits_{\Gamma_{LG}} V\left[f\,\frac{\rho\,\mathbf{v}^*}{\mu} + \gamma_2(\mathbf{v}-\mathbf{v}_0)\right]\cdot\nabla_\Gamma(\mathbf{x}'\cdot\mathbf{n})\,\mathrm{d}s \tag{33}$$

which is now consistent with the Riesz representation (20). Finally, after applying the tangential Green's formula [21, p. 367] to the term involving $\nabla_\Gamma\cdot(\mathbf{x}'\cdot\mathbf{n})$, we are able to identify the cost-functional gradients as follows

$$\nabla_\varphi\mathcal{J} = \gamma_3\varphi - T^* \quad \text{on } \Gamma_{LG}\cup\Gamma_{SG}, \tag{34a}$$
$$\nabla_{\Gamma_{LG}}\mathcal{J} = H + \kappa\mathbf{D}\cdot\mathbf{n} - \nabla_\Gamma\cdot\mathbf{D} \quad \text{on } \Gamma_{LG}, \tag{34b}$$

where

$$H = \nabla\cdot(\sigma\cdot\mathbf{v}^*) + \kappa(\nabla_\Gamma\cdot\mathbf{v}^*)\,f + \frac{\partial}{\partial n}\left[\left(\nabla_\Gamma\cdot\mathbf{v}^*\right)\,f\right] + T^*\,(\mathbf{v}-\mathbf{v}_0)\cdot\nabla T + k_L\,\nabla_\Gamma T\cdot\nabla_\Gamma T^* - \kappa\varphi\,T^*$$
$$+\gamma_3\frac{\kappa\varphi^2}{2} + \gamma_2\,V\left(\frac{\kappa V}{2}+\frac{\partial V}{\partial n}\right) + \gamma_4\left(\int\limits_{\Omega_L}\mathrm{d}x - \mathrm{Vol}_L\right),$$
$$\mathbf{D} = -V\left[f\,\frac{\rho\,\mathbf{v}^*}{\mu} + \gamma_2\,(\mathbf{v}-\mathbf{v}_0)\right].$$

We remark that using the L_2 inner product in Riesz identity (20) is not the only possibility, and in fact one may also use other inner products, for example, the Sobolev H^1 inner product which would lead to

$$\mathcal{J}'(\varphi,\Gamma_{LG};\varphi',\zeta'\mathbf{n}) = \left\langle\begin{bmatrix}\nabla_\varphi^{H^1}\mathcal{J}\\ \nabla_{\Gamma_{LG}}^{H^1}\mathcal{J}\end{bmatrix},\begin{bmatrix}\varphi'\\ \zeta'\end{bmatrix}\right\rangle_{H^1}$$
$$= \int\limits_{\Gamma_{LG}\cup\Gamma_{SG}} (\nabla_\varphi^{H^1}\mathcal{J})\varphi' + l^2\left[\nabla_\Gamma(\nabla_\varphi^{H^1}\mathcal{J})\cdot\nabla_\Gamma\varphi'\right]\mathrm{d}s \quad + \int\limits_{\Gamma_{LG}} (\nabla_{\Gamma_{LG}}^{H^1}\mathcal{J})\zeta'$$
$$+ l^2\left[\nabla_\Gamma(\nabla_{\Gamma_{LG}}^{H^1}\mathcal{J})\cdot\nabla_\Gamma\zeta'\right]\mathrm{d}s, \tag{35}$$

where $l\in\mathbb{R}^+$ is an adjustable length-scale parameter. Identifying (33) with (35), and using some identities of the tangential calculus, we arrive at

$$[I - l^2\Delta_\Gamma](\nabla_\varphi^{H^1}\mathcal{J}) = (\nabla_\varphi\mathcal{J}) \quad \text{on } \Gamma_{LG}\cup\Gamma_{SG}, \tag{36a}$$
$$\nabla_\varphi^{H^1}\mathcal{J} = 0 \quad \text{on } \partial(\Gamma_{LG}\cup\Gamma_{SG}), \tag{36b}$$
$$\left[I - l^2\Delta_\Gamma\right](\nabla_{\Gamma_{LG}}^{H^1}\mathcal{J}) = (\nabla_{\Gamma_{LG}}\mathcal{J}) \quad \text{on } \Gamma_{LG}, \tag{36c}$$
$$\nabla_{\Gamma_{LG}}^{H^1}\mathcal{J} = 0 \quad \text{on } \delta, \tag{36d}$$

where Δ_Γ is the Laplace–Beltrami operator [21, p. 365]. We thus see that, once the L_2 gradients $\nabla_\varphi\mathcal{J}$ and $\nabla_{\Gamma_{LG}}\mathcal{J}$ are determined from (34), the Sobolev H^1 gradients $\nabla_\varphi^{H^1}\mathcal{J}$ and $\nabla_{\Gamma_{LG}}^{H^1}\mathcal{J}$ can be obtained by solving elliptic boundary-value problems (36) defined on the interfaces Γ_{LG} and Γ_{SG}. As shown in [17,27], the Sobolev gradients are smoother and are useful for accelerating convergence of gradient-based optimization. These gradients will be employed in Sect. 4 to determine the optimal heat input φ and the corresponding location of the liquid–gas interface Γ_{LG}.

4 Results and discussions

In this section we present sample computations illustrating the approach developed in Sects. 2 and 3. First, we will examine the gradient fields computed based on the adjoint system (30)–(31), and then we will show how these gradients can be used to determine the optimal heat input φ and the corresponding shape of the free surface Γ_{SL}. In our approach we only need to solve the "direct" system (8)–(14) and the adjoint system (30)–(31) which is done using the finite-element method implemented in the COMSOL script environment [28]. The domains Ω_S and Ω_L are discretized using approximately 7000 unstructured tetrahedral elements with the mesh size varying from 0.04 to 0.7. In this investigation we employed only the Helmholtz, Navier–Stokes, and Arbitrary Lagrangian–Eulerian Mesh Deformation solvers, while all the other software tools, including the optimization algorithm, were implemented from scratch in the form of COMSOL scripts. In our computations we prescribed the solid–liquid interface Γ_{SL}, so that its shape and penetration depth correspond to engineering standards for good welds. The material properties used in our calculations correspond to aluminum and are collected in Table 1. As regards the dependence of the surface tension f on the temperature T [cf. relation (11)], it is known that it may be significantly affected by the presence of impurities in the alloy. As was shown in [31], in some cases their effect may be such that instead of $\mathrm{d}f(T)/\mathrm{d}T < 0$ (Table 1), one may in fact have $\mathrm{d}f(T)/\mathrm{d}T > 0$, and these modified material properties may have a far-reaching effect on the recirculating flow pattern in the weld pool. In the absence of quantitative data characterizing this effect for the material considered in this investigation (aluminum), later in this section we will model it qualitatively only by reversing the sign of the parameter A in (11). We also remark that the values of the weights $\gamma_1, \gamma_2, \gamma_3$, and γ_4 are chosen to ensure that the four terms in cost functional (15) have comparable magnitudes. The initial guesses $\{\varphi^{(0)}, \Gamma_{LG}^{(0)}\}$ for the optimization variables are

$$\varphi^{(0)}(x, y) = 4 \times 10^3 \, \mathrm{e}^{-10\,(x^2+y^2)}, \quad (x, y) \in \Gamma_{LG} \cup \Gamma_{SG}, \tag{37a}$$

$$\text{boundary } \Gamma_{LG} \text{ indicated in Fig. 1.} \tag{37b}$$

Table 1 Values of the physical and computational parameters used in the calculations [29], [30, pp. 633–651]

Physical parameter	Value
Thermal diffusivity of the solid , k_S	8.418×10^{-5} [$\mathrm{m}^2 \cdot \mathrm{s}^{-1}$]
Thermal diffusivity of the liquid, k_L	$k_S/2$ [$\mathrm{m}^2 \cdot \mathrm{s}^{-1}$]
Melting temperature, T_m	933 [K]
Ambient temperature, T_a	300 [K]
Ambient pressure, p_a	0 [Pa]
Density, ρ	2400 [$\mathrm{kg} \cdot \mathrm{m}^{-3}$]
Dynamic viscosity, μ	0.1 [$\mathrm{Pa} \cdot \mathrm{s}$]
Velocity of the heat source, U	0.01 [$\mathrm{m} \cdot \mathrm{s}^{-1}$]
Gravitational acceleration, g	9.81 [$\mathrm{m} \cdot \mathrm{s}^{-2}$]
Surface tension, $f(T)$	$10^{-3}\,(1024 - 0.274\,(T - T_m))$ [$\mathrm{N} \cdot \mathrm{m}^{-1}$]
Computational parameter	**Value**
Length-scale in Sobolev gradients, l	0.001
Weight coefficient, γ_1	10^{-5}
Weight coefficient, γ_2	1
Weight coefficient, γ_3	10^{-9}
Weight coefficient, γ_4	10^4
Vol_L	$1.04 \times$ [volume of initial weld pool shown in Fig. 1b]

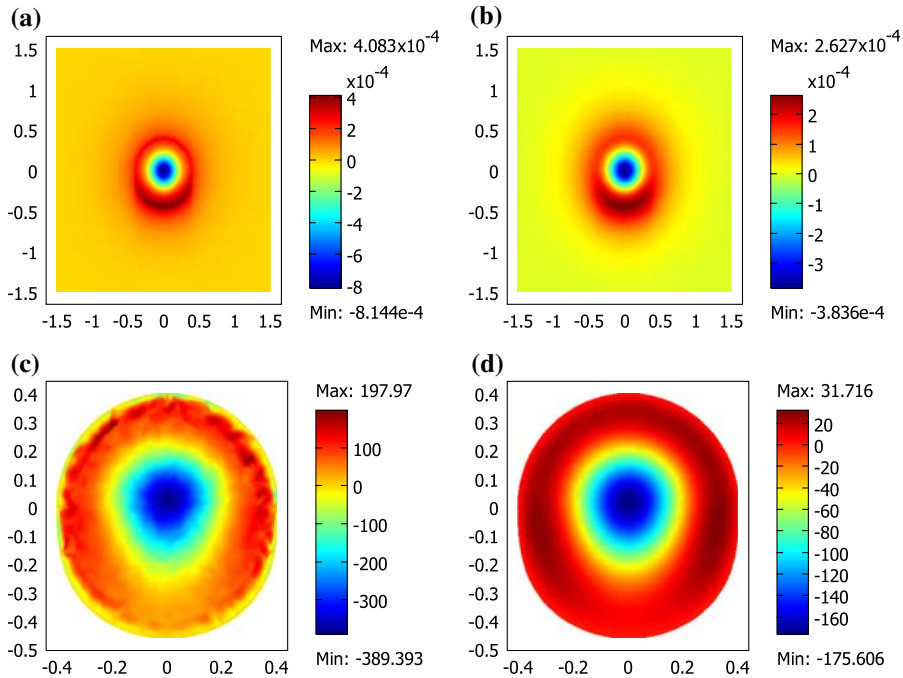

Fig. 2 Gradient fields (**a**) $\nabla_{\varphi}\mathcal{J}$, (**b**) $\nabla_{\varphi}^{H^1}\mathcal{J}$, (**c**) $\nabla_{\Gamma_{LG}}\mathcal{J}$, and (**d**) $\nabla_{\Gamma_{LG}}^{H^1}\mathcal{J}$ obtained at the first iteration

4.1 Gradients of the cost functional

Sample gradient fields $\nabla_{\varphi}\mathcal{J}$ and $\nabla_{\Gamma_{LG}}\mathcal{J}$ together with their smoothed counterparts $\nabla_{\varphi}^{H^1}\mathcal{J}$ and $\nabla_{\Gamma_{LG}}^{H^1}\mathcal{J}$ obtained at the first iteration are shown in Fig. 2. We emphasize that, while the domain of definition of these gradients includes the free surface Γ_{LG} which is not flat, for the sake of clarity in Fig. 2 we show these gradients as functions of (x, y) only. We observe that, as expected, the Sobolev H^1 gradients appear much smoother than their L_2 counterparts.

Next we proceed to demonstrate the consistency of the gradients $\nabla_{\varphi}\mathcal{J}$ and $\nabla_{\Gamma_{LG}}\mathcal{J}$ obtained using expressions (34). A standard test [32] consists in computing the Gâteaux differentials (i.e., the directional derivatives) of cost functional $\mathcal{J}(\varphi, \Gamma_{LG})$ in some arbitrary directions φ' and ζ', and comparing them to approximations of the same differentials obtained with a forward finite-difference formula. Thus, deviation of the quantities

$$\kappa_{\varphi}(\varepsilon) \triangleq \frac{\mathcal{J}(\varphi + \varepsilon\varphi', \Gamma_{LG}) - \mathcal{J}(\varphi, \Gamma_{LG})}{\varepsilon\langle\nabla_{\varphi}\mathcal{J}, \varphi'\rangle_{L_2}}, \tag{38a}$$

$$\kappa_{\Gamma_{LG}}(\varepsilon) \triangleq \frac{\mathcal{J}(\varphi, \mathbf{x}|_{\Gamma_{LG}} + \varepsilon\,\zeta'\mathbf{n}) - \mathcal{J}(\varphi, \Gamma_{LG})}{\varepsilon\langle\nabla_{\Gamma_{LG}}\mathcal{J}, \zeta'\rangle_{L_2}} \tag{38b}$$

from unity is a measure of the error. We note that an equivalent expression would be obtained using the Sobolev H^1 gradients and the associated inner products. Figures 3 and 4 illustrate the behavior of the quantities $\kappa_{\varphi}(\varepsilon)$ and $\kappa_{\Gamma_{LG}}(\varepsilon)$ as a function of the parameter ε for different combinations of the weights γ_i, $i = 1, 2, 3, 4$. These specific combinations are chosen to focus this analysis on the different terms in the cost functional $\mathcal{J}$. As regards the perturbations φ' and ζ', we choose the same form for both of them given by

$$\varphi' = \zeta' = \begin{cases} 0.1 - \sqrt{(x - x_c)^2 + (y - y_c)^2} & (x - x_c)^2 + (y - y_c)^2 < 0.01, \\ 0 & (x - x_c)^2 + (y - y_c)^2 \geqslant 0.01, \end{cases} \tag{39}$$

which is centered at $(x_c, y_c) = (0, 0)$ for the data shown in Figs. 3a and 4a, and at $(x_c, y_c) = (0.15, 0.15)$ for the data shown in Figs. 3b and 4b. We emphasize that in all cases the quantities $\kappa_{\varphi}(\varepsilon)$ and $\kappa_{\Gamma_{LG}}(\varepsilon)$ are very close to the unity for ε spanning over 10 orders of magnitude. As expected, Figs. 3 and 4 reveal an increase of the error for large

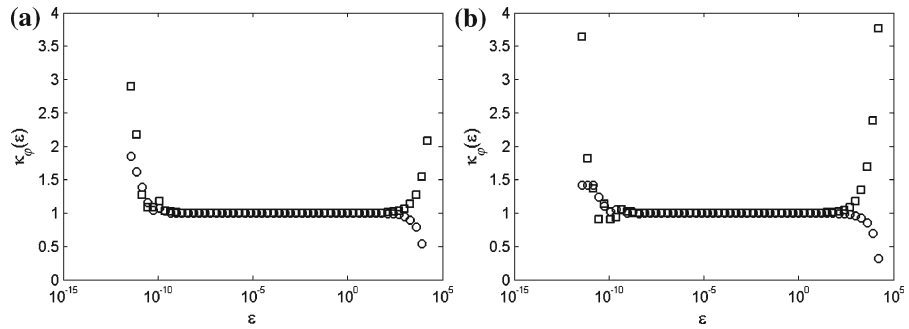

Fig. 3 The diagnostic quantity $\kappa_\varphi(\varepsilon)$ for the perturbation φ' centered at (**a**) $(0, 0)$ and (**b**) $(0.15, 0.15)$ corresponding to (*circles*) $\gamma_1 = 1,\ \gamma_2 = \gamma_3 = \gamma_4 = 0$ and (*squares*) $\gamma_2 = 1,\ \gamma_1 = \gamma_3 = \gamma_4 = 0$

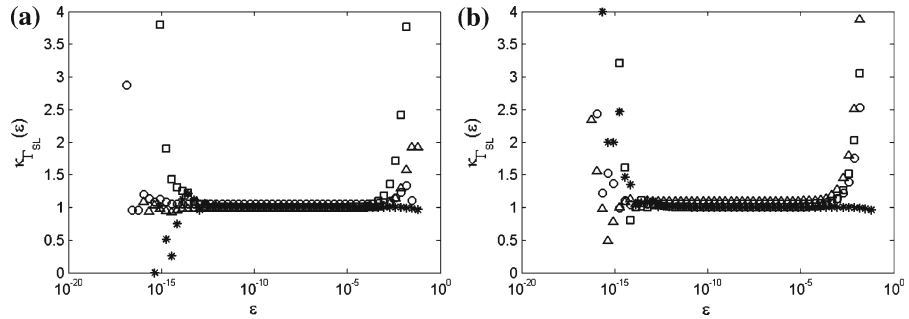

Fig. 4 The diagnostic quantity $\kappa_{\Gamma_{GL}}(\varepsilon)$ for the perturbation ζ' centered at (**a**) $(0, 0)$ and (**b**) $(0.15, 0.15)$ corresponding to (*circles*) $\gamma_1 = 1,\ \gamma_2 = \gamma_3 = \gamma_4 = 0$, (*squares*) $\gamma_2 = 1,\ \gamma_1 = \gamma_3 = \gamma_4 = 0$, (*triangles*) $\gamma_3 = 1,\ \gamma_1 = \gamma_2 = \gamma_4 = 0$, and (*asterisks*) $\gamma_4 = 1,\ \gamma_1 = \gamma_2 = \gamma_3 = 0$

values of ε, which is due to the truncations errors, and also for very small values of ε, which is due to the subtractive cancellation (round-off) errors. We emphasize that, since we are using the "optimize-then-discretize" rather than "discretize-then-optimize" approach, the gradients should not be expected to be accurate up to the machine precision [13, p. 120].

4.2 Solution of the optimization problem

Minimization procedure (4) is implemented using the steepest descent method [14, Chap. 3]. At every iteration the length of the step in the descent direction is determined using Brent's line minimization method. The following algorithm summarizes the consecutive steps in this approach:

$k \leftarrow 0$;
$\varphi^{(0)} \leftarrow$ initial guess (37a);
$\Gamma_{LG}^{(0)} \leftarrow$ initial guess (37b);
repeat
  solve direct (8)–(14) and adjoint (30)–(31) systems;
  compute gradient $\nabla_\varphi \mathcal{J}(\varphi^{(k)}, \mathbf{x}^{(k)})$;
  perform line minimization to determine the step-size $\xi^{(k)} \min_\xi \mathcal{J}\left(\varphi^{(k)} - \xi\, \nabla_\varphi \mathcal{J}(\varphi^{(k)}, \Gamma_{LG}^{(k)}), \Gamma_{LG}^{(k)}\right)$;
  update $\varphi^{(k+1)} = \varphi^{(k)} - \xi^{(k)}\, \nabla_\varphi \mathcal{J}(\varphi^{(k)}, \Gamma_{LG}^{(k)})$;
  solve direct (8)–(14) and adjoint (30)–(31) systems;
  compute gradient $\nabla_{\Gamma_{LG}} \mathcal{J}(\varphi^{(k+1)}, \Gamma_{LG}^{(k)})$;

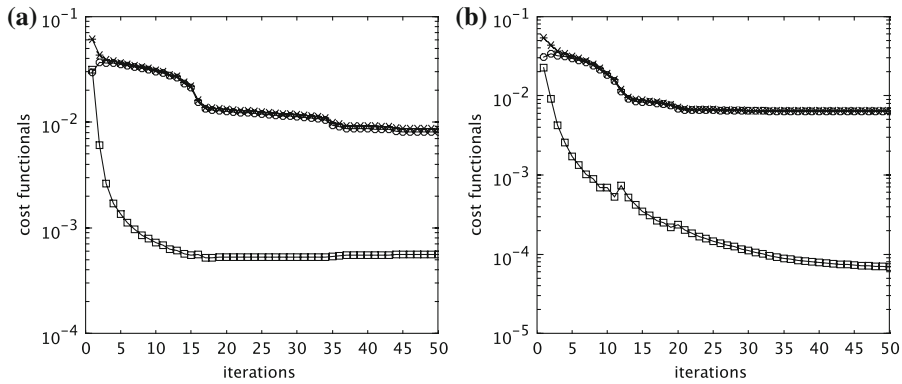

Fig. 5 Cost functionals as a function of the number of iterations for the case (**a**) $\mathrm{d}f(T)/\mathrm{d}T < 0$ and (**b**) $\mathrm{d}f(T)/\mathrm{d}T > 0$ with (*asterisks*) total functional $\mathcal{J}$, (*circles*) $\gamma_1\mathcal{J}_1 + \gamma_3\mathcal{J}_3$, and (*boxes*) $\gamma_2\mathcal{J}_2 + \gamma_4\mathcal{J}_4$ [cf. (15)]

perform line minimization to determine the step-size $\eta^{(k)} \min_{\eta} \mathcal{J}\left(\varphi^{(k+1)}, \mathbf{x}|_{\Gamma_{LG}^{(k)}} - \eta\, \nabla_{\Gamma_{LG}} \mathcal{J}(\varphi^{(k+1)}, \Gamma_{LG}^{(k)})\right)$;

update Γ_{LG} by deforming it along the direction $\nabla_{\Gamma_{LG}} \mathcal{J}(\varphi^{(k+1)}, \Gamma_{LG}^{(k)})$ with the step size $-\eta^{(k)}$;

$k \leftarrow k + 1$;

until $\max(|\xi^{(k)}|, |\eta^{(k)}|) < \varepsilon_\tau$,

where ε_τ is a prescribed tolerance. We note that the descent steps for the control variables φ and Γ_{LG} are performed independently. The reason for this is that the part of the problem related to the optimization of the shape of the free surface Γ_{LG} is "stiffer" than the part related to the optimization of the heat input φ; hence the two parts are characterized by quite different rates of convergence. Furthermore, we also observed that iterations can be significantly accelerated if we set $\gamma_2 = \gamma_4 = 0$ during the substep involving minimization with respect to φ, and $\gamma_1 = \gamma_3 = 0$ during the substep involving minimization with respect to Γ_{LG}. This strategy was used to obtain the results reported below.

Figure 5 shows the decrease of cost functional (15) and its constituent terms as a function of the number of iterations. We observe that the proposed algorithm results in a steady convergence despite the complicated nature of the problem, although the rate of convergence is relatively slow (essentially linear). We also note that in both cases the terms $\gamma_2\mathcal{J}_2 + \gamma_4\mathcal{J}_4$ reach a very low level which confirms that the problem of determining a steady free surface Γ_{SL} is solved with a sufficient accuracy. Different numbers of iterations required by $\gamma_1\mathcal{J}_1 + \gamma_3\mathcal{J}_3$ and $\gamma_2\mathcal{J}_2 + \gamma_4\mathcal{J}_4$ to reach a plateau illustrate the different rates of convergence characterizing optimization of the heat input φ and the location of the free surface Γ_{LG}. Next, in the following figures we examine certain features of the solutions obtained when the iterations have converged. In Figs. 6 and 8 we show the distribution of the temperature T in three different cross-sections of the weld pool and the workpiece in addition to the optimal distribution of the heat flux φ on the top surface $\Gamma_{LG} \cup \Gamma_{SG}$ for the problems with $\mathrm{d}f(T)/\mathrm{d}T < 0$ and $\mathrm{d}f(T)/\mathrm{d}T > 0$. In Figs. 7 and 9 we show the velocity vector fields in two cross-sections of the weld pool for the same two cases with $\mathrm{d}f(T)/\mathrm{d}T < 0$ and $\mathrm{d}f(T)/\mathrm{d}T > 0$. In Figs. 7 and 9 we also include the velocity vector fields corresponding to the initial guess $\{\varphi^{(0)}, \Gamma_{LG}^{(0)}\}$. By comparing these initial guesses with the converged solutions, one can see a significant decrease in the magnitude of the normal velocity components on the free surface Γ_{LG} which indicates that our algorithm indeed converges to a steady boundary. The relatively slow rate of convergence observed in Fig. 5 can be explained by a rather modest resolution of the finite-element mesh in the narrow wedge regions in the vicinity of the contact line. This affects the accuracy with which the gradient terms involving partial derivatives of state variables can be evaluated in expressions (34). Remarkably, by comparing the flow patterns obtained in the cases with $\mathrm{d}f(T)/\mathrm{d}T < 0$ and $\mathrm{d}f(T)/\mathrm{d}T > 0$ (Figs. 7c,d, 9c,d), we note that the recirculating motion in the weld pool has opposite direction in the two cases. This interesting feature of this problem was discussed in detail in [31] (see their Fig. 18), and it is encouraging to see it is captured by our approach.

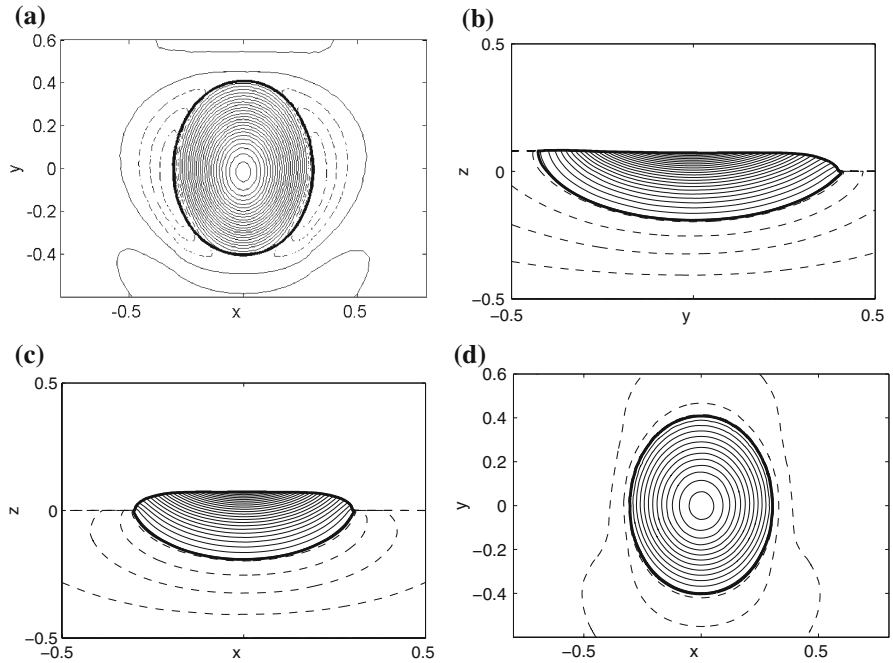

Fig. 6 Case with $\mathrm{d}f(T)/\mathrm{d}T < 0$: (**a**) optimal heat flux φ on $\Gamma_{LG} \cup \Gamma_{SG}$ and the corresponding temperature T distributions in the cross-sectional planes with (**b**) $x = 0$, (**c**) $y = 0$, and (**d**) $z = 0$; in (**a**) the heat flux increment between neighboring isolines is 500 [deg · m · s^{-1}]; in (**b–d**) the temperature increment between neighboring isolines is 150 [deg]; the *solid* and *dashed lines* correspond to, respectively, $\varphi > 0$ and $\varphi < 0$ in (**a**), and to $T > T_m$ and $T < T_m$ in (**b–d**); for clarity, isolines are not drawn in areas with steep temperature gradients

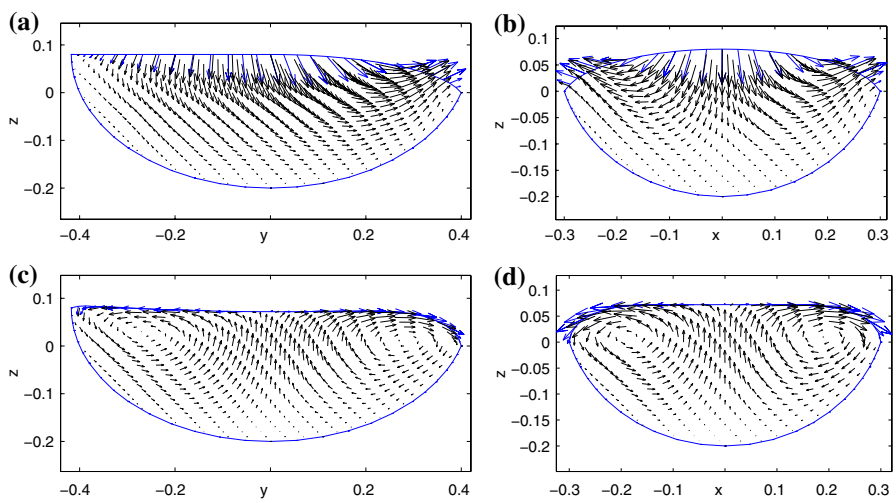

Fig. 7 Case with $\mathrm{d}f(T)/\mathrm{d}T < 0$: the velocity fields corresponding to (**a**, **b**) the initial guess and (**c**, **d**) the converged solution in the cross-sectional planes with (**a**, **c**) $x = 0$ and (**b**, **d**) $y = 0$

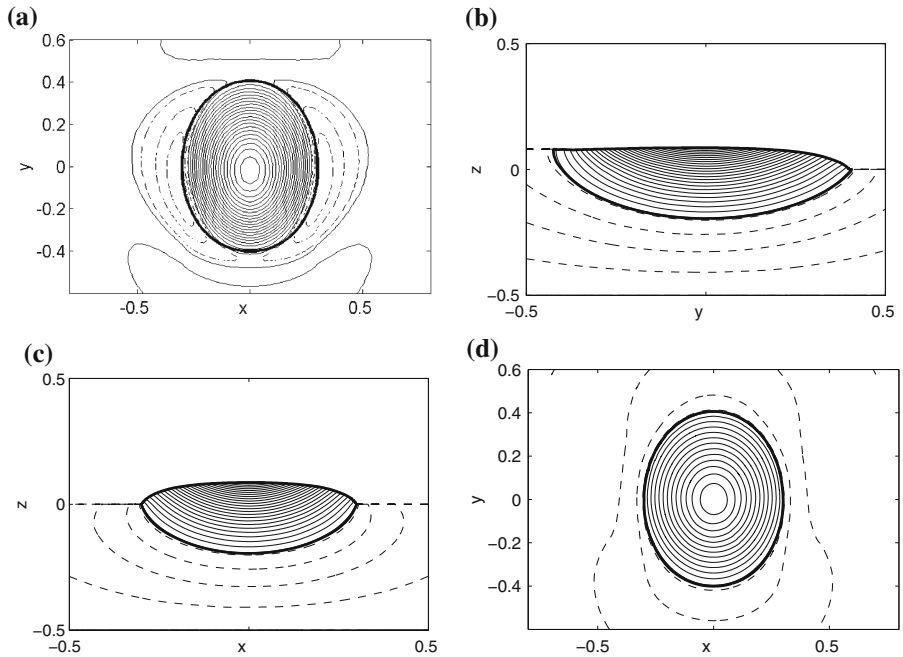

Fig. 8 Case with $\mathrm{d}f(T)/\mathrm{d}T > 0$: (**a**) optimal heat flux φ on $\Gamma_{LG} \cup \Gamma_{SG}$ and the corresponding temperature T distributions in the cross-sectional planes with (**b**) $x = 0$, (**c**) $y = 0$, and (**d**) $z = 0$; in (**a**) the heat flux increment between neighboring isolines is 500 [deg · m · s^{-1}]; in (**b–d**) the temperature increment between neighboring isolines is 150 [deg]; the *solid* and *dashed lines* correspond to, respectively, $\varphi > 0$ and $\varphi < 0$ in (**a**), and to $T > T_m$ and $T < T_m$ in (**b–d**); for clarity, isolines are not drawn in areas with steep temperature gradients

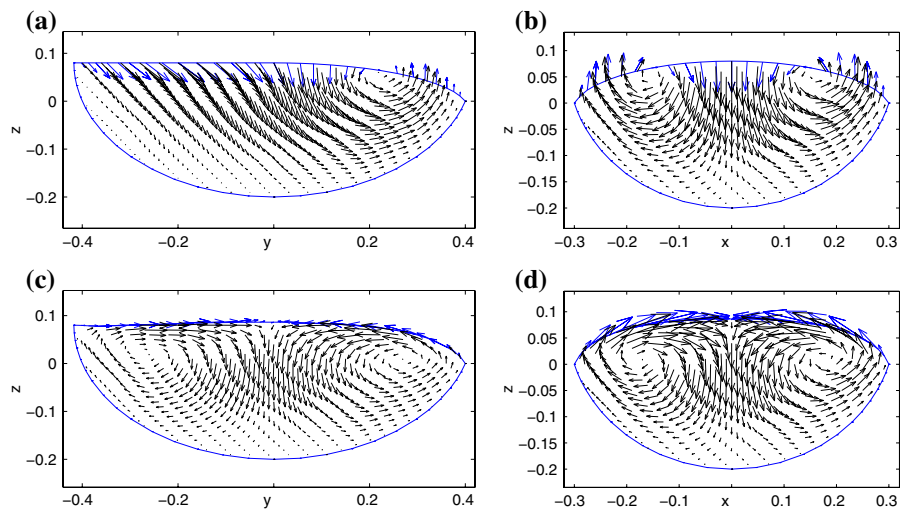

Fig. 9 Case with $\mathrm{d}f(T)/\mathrm{d}T > 0$: the velocity fields corresponding to (**a**, **b**) the initial guess and (**c**, **d**) the converged solution in the cross-sectional planes with (**a**, **c**) $x = 0$ and (**b**, **d**) $y = 0$

5 Conclusions

In this work we solved an optimization problem for a welding process involving convection of liquid metal and characterized by a complex interplay of a number of physical effects. This was achieved by developing a unified approach to solving free-boundary and inverse problems in the steady-state regime. We did this by formulating this

problem as PDE-constrained optimization. Advantages of such an inverse formulation of a free-boundary problem analogous to the present one were discussed in [17]; see also [16] for a more general perspective. In the present investigation we generalized this methodology by also performing optimization of actual control inputs, here the heat flux φ. Our work demonstrates that these techniques can be successfully implemented numerically providing quite encouraging computational results despite the complexity of the geometry and nonlinearity of the governing equations. We envision a number of ways in which the approach developed in this paper can be further extended. Firstly, one can incorporate a more accurate model for the interaction of the weld pool surface with the heat source. Such a higher-fidelity model accounting for electromagnetic effects due to the presence of an electric arc and plasma above the weld pool is already being implemented and the results will be reported separately. We also note that the value of the dynamic viscosity μ used in our calculations (Table 1) is somewhat higher than the actual value. The reason is that using the actual value would result in a higher Reynolds number which would require a significantly finer mesh than what we can currently afford with our computational resources. On the other hand, we remark that this increased viscosity might be interpreted as an "eddy viscosity" which is consistent with our formulation of the problem as an idealized model for *statistically* steady solutions in the moving frame of reference. In our future work we are planning to elaborate this aspect of our approach by incorporating a "proper" turbulence model consistent with the use of an eddy viscosity. A related question concerns the stability of the computed solutions, in particular, for higher Reynolds numbers. Another important challenge concerns the generalization of our present approach to time-dependent problems. We note that cost functional gradients for free-boundary problems defined in such settings can be derived using the "non-cylindrical calculus" [33, pp. 114–118] which provides a generalization of the shape calculus to time-dependent problems. We are currently investigating these issues and some preliminary results concerning adjoint-based optimization of unsteady free-boundary problems using some simple model systems were already reported in [15].

Acknowledgments The authors acknowledge interesting discussions with John Lowke, Arian Novruzi and Tony Murphy. We also wish to thank the Natural Sciences & Engineering Research Council of Canada (NSERC), McMaster Centre for Automotive Materials & Manufacturing (MCAMM), Ontario Centres of Excellence—Centre for Materials and Manufacturing (OCE–CMM) and General Motors of Canada for generous support provided for this research.

References

1. Lancaster JF (1986) The physics of welding. Pergamon Press, Oxford
2. Na S-J, Lho T-J (1996) A study on parameter optimization for circumferential gas tungsten arc (GTA) welding of small pipes considering backing gas pressure. Part 2: process optimization. Proc Inst Mech Eng 210:87–91
3. Kim D, Rhee S (2001) Optimization of arc welding process parameters using a genetic algorithm. Weld J 80:184–189
4. De A, DebRoy T (2006) Improving reliability of heat and fluid flow calculations during conduction model laser spot welding by multi-variable optimization. Sci Technol Weld Join 11:143–153
5. Zabaras N (1998) Adjoint methods for inverse free convection problems with application to solidification processes. In: Borggaard J, Cliff E, Schreck S, Burns J (eds) Computational methods for optimal design and control (Birkhauser series in progress in systems and control theory). Birkhauser, New York, pp 391–426
6. Hinze M, Ziegenbald S (2007) Optimal control of the free boundary in a two-phase Stefan problem. J Comput Phys 223:657–684
7. Dowden JM (2001) Mathematics of thermal modelling: an introduction to the theory of laser material processing. CRC Press, Boca Raton
8. Wang Y, Tsai HL, Martin SP, Wang PC (2002) Modeling heat and mass transfer and fluid flow in three-dimensional gas metal arc welding. In: Proceedings of IMECE 2002
9. Zhao PC, Wu CS, Zhang YM (2004) Numerical simulation of the dynamic characteristics of weld pool geometry with step changes of welding parameters. Model Simul Mater Sci Eng 12:765–780
10. Bewley TR (2001) Flow control: new challenges for a new renaissance. Prog Aerosp Sci 37:21–58
11. Kalnay E (2003) Atmospheric modeling, data assimilation and predictability. Cambridge University Press, New York
12. Cerviño LI, Bewley TR, Freund JB, Lele SK (2002) Perturbation and adjoint analyses of flow-acoustic interactions in an unsteady 2D jet. In: Center for turbulence research, proceedings of the summer program 2002, pp 27–40
13. Gunzburger MD (2003) Perspectives in flow control and optimization. SIAM, Philadelphia
14. Nocedal J, Wright S (2002) Numerical optimization. Springer, New York
15. Protas B, Liao W (2008) Adjoint-based optimization of PDEs in moving domains. J Comput Phys 227:2707–2723

16. Neittaanmaki P, Sprekels J, Tiba D (2006) Optimization of elliptic systems: theory and applications. Springer, Berlin
17. Volkov O, Protas B (2009) An inverse model for a free-boundary problem with a contact line: steady case. J Comp Phys (in press)
18. Gurtin ME (1993) Thermomechanics of evolving phase boundaries in the plane. Oxford University Press, Oxford
19. Engl H, Hanke M, Neubauer A (1996) Regularization of inverse problems. Kluver, Dordrecht
20. Sokolowski J, Zolésio J-P (1992) Introduction to shape optimization: shape sensitivity analysis. Springer, Berlin
21. Delfour MC, Zolésio J-P (2001) Shape and geometries—analysis, Differential Calculus and Optimization. SIAM, Philadelphia
22. Haslinger J, Mäkinen RAE (2003) Introduction to shape optimization: theory, approximation and computation. SIAM, Philadelphia
23. Mohammadi B, Pironeau O (2004) Shape optimization in fluid mechanics. Annu Rev Fluid Mech 36:255–279
24. Simon J (1980) Differentiation with respect to domain in boundary value problems. Numer Funct Anal Optim 2(7&8):649–687
25. Berger MS (1977) Nonlinearity and functional analysis. Academic Press, New York
26. Adams RA, Fournier JF (2005) Sobolev spaces. Academic Press, New York
27. Protas B, Bewley T, Hagen G (2004) A comprehensive framework for the regularization of adjoint analysis in multiscale PDE systems. J Comput Phys 195(1):49–89
28. See www.comsol.com
29. Sarou-Kanian V, Millot F, Rifflet JC (2003) Surface tension and density of oxygen-free liquid aluminum at high temperature. Int J Thermophys 24:277–286
30. Holman JP (2002) Heat transfer. McGraw-Hill, New York
31. Tanaka M, Lowke JJ (2007) Predictions of weld pool profiles using plasma physics. J Phys D 40:R1–R23
32. Homescu C, Navon IM, Li Z (2002) Suppression of vortex shedding for flow around a circular cylinder using optimal control. Int J Numer Meth Fluids 38:43–69
33. Moubachir M, Zolésio J-P (2006) Moving shape analysis and control—applications to fluid structure interactions. Chapman & Hall, Boca Raton